IEEE Access
Multidisciplinary ⋮ Rapid Review ⋮ Open Access Journal

Received 5 July 2024, accepted 8 August 2024, date of publication 16 August 2024, date of current version 29 August 2024.

Digital Object Identifier 10.1109/ACCESS.2024.3445175

RESEARCH ARTICLE

On the Field Statistics in Nested Reverberation Chambers

ANGELO GIFUNI[1], (Member, IEEE), ANETT KENDERES[2], GIUSEPPE GRASSINI[1], ANDREA BUONO[1], (Senior Member, IEEE), AND GABRIELE GRADONI[3], (Member, IEEE)

[1]Dipartimento di Ingegneria, Università degli Studi di Napoli "Parthenope," 80143 Naples, Italy
[2]Department of Broadband Infocommunications and Electromagnetic Theory, Budapest University of Technology and Economics, H-1111 Budapest, Hungary
[3]Institute for Communication Systems, University of Surrey, Surrey, GU2 7XH Guildford, U.K.

Corresponding author: Angelo Gifuni (angelo.gifuni@uniparthenope.it)

This work was supported in part by the Doctoral Student Scholarship Program funded by the Cooperative Doctoral Program of the Ministry for Innovation and Technology from the National Research Development and Innovation Fund, and in part by the Hungarian Scientific Research Fund under Grant K-135307.

ABSTRACT We study the normalized field statistics inside nested reverberation chambers (NRCs), through the analysis of the shielding effectiveness of enclosures and material samples. The accurate knowledge of field statistics allows to improve the estimation of probability distributions for high field values inside electrically large enclosures. Furthermore, the study allows for better selection of the measurement model for both shielding effectiveness of enclosures and materials and gaskets. We find the correct procedures to achieve such distributions. We study basic cases of single and electrically small coupling apertures filtering single or double field components and we show the theoretical statistics of the field components inside NRCs. The change of inner field distributions is driven by the electrical size of coupling apertures and has been verified experimentally. The theory developed to obtain such statistics is based upon physics and the results are supported by measurements. The procedures and results shown in this paper are applicable to predict the statistics in NRCs as well as in adjacent RCs.

INDEX TERMS Nested reverberation chamber, stochastic electromagnetic fields, electromagnetic coupling, shielding effectiveness measurements.

I. INTRODUCTION

Reverberation chambers (RCs) have become an important facility for EMC testing [1], as well as for wireless device testing [2], [3], [4]. Several specific standardized tests are performed by RCs, nested RCs (NRCs) and adjacent RCs (ARCs). Shielding effectiveness (SE) of enclosures [5], [6], [7], [8], [9], [10], [11], [12], as well as of materials and gaskets can be measured by NRCs [1], [13], [14], [15], [16], and/or ARCs [17], [18]. NRCs and ARCs are systems of two RCs coupled with each other by one or more apertures. In the former case, a smaller chamber is positioned inside a larger chamber. An accurate knowledge of the distributions of the single field components inside the inner chamber for NRCs and inside the chamber that is fed by the other chamber for ARCs entails an accurate prediction of the probability of high values of field that can occur inside the enclosures [19] or the other chamber for ARCs, for both single components and total field [1], [20], [21]. Generally, a single component of the field is received by an unintentional receiver (parts of circuits, components, or an electrical system in immunity tests). In [19], a study on the maximum field distribution in an NRC was addressed by considering a generalized extreme distribution, which does not require the knowledge of the distribution of the field inside the inner chamber. Moreover, the accurate knowledge of the distributions inside the inner chamber in the measurements of SE of materials allows a better measurement quality and selection of the measurement model for both SE of materials and gaskets [1], [22, Subsect. II-D] and of enclosures [1], [23].

The two chambers are considered to be sufficiently isolated so that the correspondent inner fields are assumed independent of each other [13], [14], [16]. The study performed in this paper entails the knowledge of the distributions of the

The associate editor coordinating the review of this manuscript and approving it for publication was Mahmoud A. Abdalla.

fields inside the two coupled chambers, when they operate in a standalone way. In this paper, ''standalone way'' strictly means that the signal is transmitted and received in the same chamber with the same configuration of coupling between the chambers. A χ distribution with two degrees of freedom (2 DOFs, also called Rayleigh distribution) is assumed for the amplitude of each field component in both the chambers, when they operate in a standalone way. Such a distribution is achieved when the fields are well-stirred [24], [25]. The theoretical models we show are valid for both NRCs and ARCs. However, we have experimental availability of an in-house NRCs. We are interested in the distributions of the field components normalized with respect to their mean values. The field is often compared (normalized) to the average value so that it is important to know the behaviour of the PDFs for values greater than the mean value.

In the literature, numerous studies on the distribution of the maximum field inside complex cavities are present [20], [21]. However, to the best of our knowledge, the literature on field statistics in NRCs is rather limited. In addition to the recent study in [19], there are two papers: one on measurements [26] and another on theory [27]. In [28, Table 2], some results were shown for a large coupling aperture, which actually conflict with the theory in [27]. In [26], rectangular coupling apertures of different sizes were tested, in order to observe the change of the distribution of the field components inside the enclosure[1] without justifying the choice of the form of such apertures. Nonnormalized values of the field were considered. A double-Rayleigh distribution of the field components was observed for the smaller coupling aperture used in the measurements, even though the authors specify that further research were necessary to clarify some anomaly observed in the results [26, Subsection *B*]. However, only the sizes of the coupling apertures were highlighted while the effect of their form was not mentioned, i.e., only the isolation between the chambers was considered. In short, in [26], only the double-Rayleigh was assumed for the distribution of the components of the filed inside the enclosure regardless of the form of the aperture. In [27], only cases where the χ^2 distribution with 2 DOFs were considered for the power transmitted into the inner chamber. No consideration on size and form of the coupling aperture and on the possible consequent filtering behaviour was shown. In [27], the probability density function (PDF) and related cumulative distribution function (CDF) of the field components inside the inner chamber was derived from the normalized received power inside the inner chamber by a simple transformation [27, eq. (10)]. The power was normalized to the average value [27, eq. (7)]. In this way, no correct distribution of the field can be obtained as such a normalization inhibits the correct above-mentioned transformation; accordingly, the achieved PDF and CDF of the field are not correct for any geometry of the coupling aperture [27, eqs. (11) and (12)]. For the sake of clarity, we specify that the PDF and CDF of the normalized power to the average value derived in [27, eqs. (8) and (9)] is only valid for one-dimensional (1D) electrically small (ES) coupling apertures as shown below; however, the authors in [27] were unaware of such a restriction and they did not mention it.

In [28, Sect. II and Table 2], it is still *de facto* assumed that only a good isolation between the chambers is sufficient to achieve a double Rayleigh distribution of the field components inside the inner chamber for NRCs or in the other chamber for ARCs without considering the size and the form of the coupling aperture.

However, it is necessary to shed light on the field statistics in the NRCs, as well as ARCs and to enhance them for the effect of different forms of ES coupling apertures, which is not considered in the literature.

The distributions of fields and powers can be achieved for both nonnormalized and normalized values of fields and powers. Since, we are interested in the distributions of the field components normalized with respect to their mean values, we show the procedure to achieve such normalized distributions of each field components inside the inner chamber, which has the same form as the distribution of the amplitude of the transmission coefficient ($|S_{21}|$) measured between the chambers. The filtering behaviour due to the geometry of the aperture is considered. We accurately study the effect of ES coupling apertures on the statistics of the amplitude of the field components of NRCs and ARCs. Hence, individual small coupling apertures between the two chambers have to be treated separately if the spatial filtering pertains one or two field planar components. Such a spatial filtering corresponds to the 1D and two-dimensional (2D) cases of ES coupling apertures, respectively. A single and ES coupling aperture *de facto* implies the independence between fields inside the two coupled RCs. It is important to note that coupling apertures can be considered ''ES'' until the frequencies in the resonance region of the aperture itself where the amplitude and phase of the field on the aperture can still be considered approximately constant. It is specified that the use of a single very ES aperture in the measurements can be tricky as the leakage could affect the measurements quality.

However, we derive the theoretical distributions by a physical and formal reasoning, i.e., they are not simple statistical assumptions (null hypothesis to be tested).

When more than one ES aperture is present, their effects can properly be summed; the mutual coupling has to be considered if they are not independent [27]. As the number of the ES apertures increases and/or as the aperture size increases, the distribution of the amplitude of the field components inside the nested chamber gradually converges to a χ distribution with 2 DOFs [24], [27] regardless of the independence of the fields inside the coupled chambers. This is true for a single aperture as well. Note that an electrically large (EL) aperture can be considered as a special case of many apertures [27].

[1]Note that we use the words ''inner chamber'' and ''enclosure'' interchangeably [1].

The paper is organized as follows: in Section II, the theory is developed; in Section III, the measurement setup and data acquisition are shown; in Section IV, results are provided while in Section V, they are discussed. In Section VI, conclusions are drawn.

II. THEORY AND COMPARISON METHODS

In this section, we consider specific ES coupling apertures between the chambers and develop the theory to achieve the distributions of the field components inside the inner chamber. Even though the theory is the same for both NRCs and ARCs as mentioned above, we henceforth mention only NRCs for ease. As mentioned above, it is assumed that each field component has a χ distribution with 2 DOFs inside each of the two chambers of the NRCs system, when they operate in a standalone way. A sketch representing the NRCs system is shown in Fig. 1. It is specified that the subscript o (i) means outer (inner) chamber. The subscripts o (i) could be replaced with different subscripts when ARCs are considered.

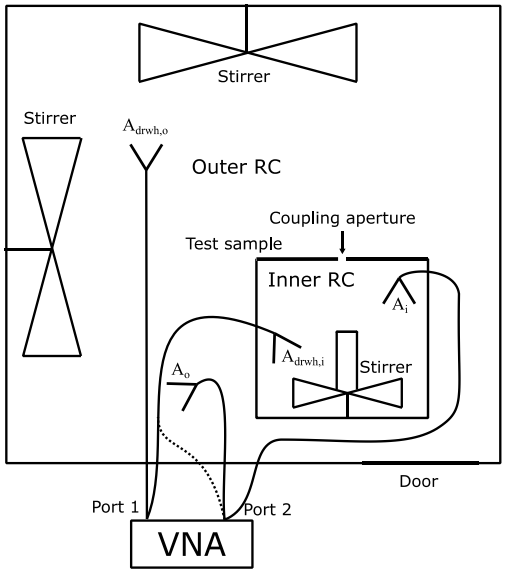

FIGURE 1. Sketch of measurement setup.

A. SINGLE ES APERTURES FILTERING A SINGLE FIELD COMPONENT (1D CASES)

In this subsection, a single 1D ES aperture, which filters a single component of the incident field, is considered. In the measurements, single ES rectangular slots were used. For such cases, the amplitude of the field transmitted inside the inner chamber through the small aperture has a χ distribution with 2 DOFs [24]. The field transmitted from the outer chamber is subject to the stirring inside the inner chamber. Therefore, the transmitted field component is subject to a χ distribution with 2 DOFs inside the inner chamber again. Accordingly, each field component measured inside the inner chamber, which is a random variable (RV) denoted by X, is achieved by the product of two RVs, which are denoted by X_1 and X_2, respectively. The latter (X_1 and X_2) have a χ distribution with 2 DOFs. The distribution of the amplitude of each field component has double Rayleigh profile inside the inner chamber, which is achieved by the product of two Rayleigh distribution. We derive the normalized PDF and the CDF of the amplitude of the transmission coefficient between the chambers $|S_{21,o,i}|$, which have the same shape as those of the amplitude of the field received by an antenna. The PDF and CDF of the square of the amplitude of the transmission coefficient between the chambers $\left(|S_{21,o,i}|^2\right)$, which have the same shape as those of the received power, are not derived for this case because they are as those derived in [27], even though no mention on the shape filtering of the geometry of the coupling aperture is found in [27].

We denote by P_a the power transmitted through the coupling aperture. We can consider the coupling aperture represented by two virtual back-to-back antennas, one in one chamber and one in the other chamber. Note that the virtual antennas can be considered as linearly polarized in cases of 1D coupling apertures, whereas they can be considered as circularly polarized in cases of 2D coupling apertures. We denote by P_t and P_r the power transmitted by the transmitting antenna inside the outer chamber and that received by the receiving antenna inside the inner chamber, respectively. These powers are connected to the fields $\underline{E_t}$, $\underline{E_r}$, and $\underline{E_a}$. We consider the amplitudes of the transmission coefficients related to such fields and powers by writing:

$$|S_{21}|_a = \frac{|\underline{E_a}|}{|\underline{E_t}|} = \frac{\sqrt{P_a}}{\sqrt{P_t}} = X_1 \tag{1}$$

$$|S_{21}|_r = \frac{|\underline{E_r}|}{|\underline{E_a}|} = \frac{\sqrt{P_r}}{\sqrt{P_a}} = X_2 \tag{2}$$

where $|S_{21}|_a$ and $|S_{21}|_r$ are respectively the amplitudes of the transmission coefficients of the outer chamber including the attenuation though the aperture, which receives and transmits the power P_a, and of the inner chamber. $|\underline{E_t}|$ and $|\underline{E_r}|$ are the amplitudes of the fields at the reference planes of the transmitting and receiving antennas, respectively, whereas $|\underline{E_a}|$ is the amplitude of the field at the reference plane of the virtual antenna inside the enclosure. Note that $|\underline{E_a}|$ is reduced by the attenuation of the coupling aperture and that the reference plane concerning $|\underline{E_t}|$ and $|\underline{E_r}|$ corresponds to the calibration plane of the measurements. We consider the amplitude of the transmission coefficient:

$$|S_{21,o,i}| = \frac{|\underline{E_r}|}{|\underline{E_t}|} = \frac{\sqrt{P_a}}{\sqrt{P_t}}\frac{\sqrt{P_r}}{\sqrt{P_a}} = \frac{\sqrt{P_r}}{\sqrt{P_t}} = X = X_1X_2 \tag{3}$$

which represents the RV X.

The PDFs of X_1 and X_2 can respectively be expressed as follows:

$$f_{X_1}(x_1) = \frac{x_1}{\sigma_1^2} e^{-\frac{x_1^2}{2\sigma_1^2}} \tag{4}$$

$$f_{X_2}(x_2) = \frac{x_2}{\sigma_2^2} e^{-\frac{x_2^2}{2\sigma_2^2}} \tag{5}$$

where σ_1^2 and σ_2^2 are the variances of the Gaussian components of the related field components. It is specified that the subscripts of the variances σ_1^2 and σ_2^2 are different from the subscripts o (i) as σ_1^2 or σ_2^2 includes the attenuation through the aperture due to the mismatches of the two virtual antennas, which is denoted by A_{ca}. Note that, the transmission coefficients are reciprocal; we can consider that σ_1^2 includes A_{ca}. The attenuation through the coupling mechanism between the chambers can be assumed constant, i.e., it changes only if the frequency changes. Note that it limits the use of frequency stirring (FS). It is worth noting that the attenuation A_{ca} could be estimated by measurements [22], or by calculations [29], [30], [31]. However, σ_1 and σ_2 can also be estimate by measurements.

The mean values of X_1 and X_2 are $\mu_{X_1} = \frac{\sqrt{2\pi}}{2}\sigma_1$ and $\mu_{X_2} = \frac{\sqrt{2\pi}}{2}\sigma_2$, respectively. Therefore, we can write:

$$X_{1n} = \frac{X_1}{\mu_{X_1}} \tag{6}$$

$$X_{2n} = \frac{X_2}{\mu_{X_2}}. \tag{7}$$

We specify that the subscript "n" means normalized throughout the paper.

Accordingly, we obtain:

$$f_{X_{1n}}(x_1) = \frac{\pi}{2} x_{1n} e^{-\frac{\pi x_{1n}^2}{4}} \tag{8a}$$

$$f_{X_{2n}}(x_2) = \frac{\pi}{2} x_{2n} e^{-\frac{\pi x_{2n}^2}{4}}. \tag{8b}$$

Clearly, the PDF of X_{2n} is the same as that of X_{1n}.

We are interested in the PDF and the CDF of the normalized RV

$$X_n = X_{1n} X_{2n} = \left|S_{21,o,i}\right|_n \tag{9}$$

where X_{1n} and X_{2n} are independent. We achieve:

$$f_{X_n}(x_n) = \left(\frac{\pi}{2}\right)^2 x_n K_0\left(\frac{\pi}{2} x_n\right) \tag{10}$$

$$F_{X_n}(x_n) = 1 - \frac{\pi}{2} x_n K_1\left(\frac{\pi}{2} x_n\right) \tag{11}$$

where K_0 and K_1 are the modified Bessel functions of second kind and of zeroth and firth order, respectively. Equations (10) and (11) were achieved using the theory on the statistical distribution of the product between two independent RVs [32].

It is worth comparing (10) and (11) with the corresponding expressions (11) and (12) in [27]. Figure 2 shows the plot of PDF in (10) along with some PDF comparisons.

We can note that the tail of the PDF (10), which is a normalized double Rayleigh, is fatter than both PDF [27, eq. (11)] and normalized χ with 2 DOFs. We specify that the PDF [27, eq. (11)] *de facto* corresponds to a nonnormalized double Rayleigh, whose scale parameter $\sigma = \sigma_1\sigma_2$ is equal to $1/2$ [26] and the mean value is equal to $\pi/4$. Indeed, the

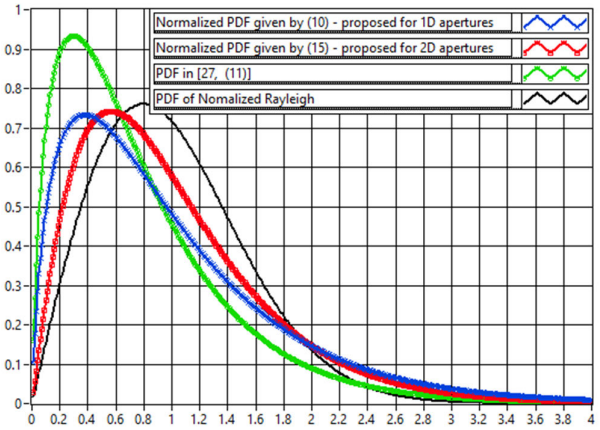

FIGURE 2. PDFs. The blue-coloured and cross-marked trace is the normalized PDF (10), which is a Double Rayleigh; red-coloured and square-marked trace is the normalized PDF (15); green-coloured and circle-marked trace is the PDF [27, eq. (11)]; black-coloured and unmarked trace is the normalized χ with 2 DOFs.

PDF of a nonnormalized RV X, which has a double Rayleigh distribution, is [26]:

$$f_X(x) = \frac{x}{(\sigma_1\sigma_2)^2} K_0\left(\frac{x}{\sigma_1\sigma_2}\right) \tag{12}$$

where $\sigma_1\sigma_2$ is the scale parameter of the data [26].

B. SINGLE ES APERTURES FILTERING TWO FIELD COMPONENTS (2D CASES)

In this subsection, a single 2D ES aperture, which filters two components of the incident field, is considered. In the measurements, single ES circular apertures were used for ease of the practical realization. In these cases, the amplitude of the field transmitted inside the inner chamber has a χ distribution with 4 DOFs [33], [34]. Indeed, two random field components require four independent Gaussian distributions in complex representation, whose amplitude has the abovementioned distribution. Accordingly, each field component measured inside the inner chamber is achieved by taking the product of two RVs, of which one has a χ distribution with 4 DOFs [33], [34] and the other has a χ distribution with 2 DOFs; we denote them by Y_1 and X_2, respectively. We are now interested in the PDF and CDF of the normalized RV

$$Y_n = Y_{1n} X_{2n} = \left|S_{21,o,i}\right|_n. \tag{13}$$

The PDF of X_{2n} is given by (8b) whereas the PDF of Y_{1n} is given by

$$f_{Y_{1n}}(y_{1n}) = \frac{81\pi^2}{128} y_{1n}^3 e^{-\frac{9\pi}{16} y_{1n}^2}. \tag{14}$$

The PDF and CDF of Y_n turn out to be, respectively:

$$f_{Y_n}(y_n) = \frac{27\pi^3}{128} y_n^2 K_1\left(\frac{3\pi}{4} y_n\right) \tag{15}$$

$$F_{Y_n}(y_n) = 1 - \frac{9\pi^2}{32} y_n^2 K_2\left(\frac{3\pi}{4} y_n\right) \tag{16}$$

where K_2 is the modified Bessel functions of second kind and of second order.

Fig. 2 shows a comparison between the plots of PDFs (10), (15), [27, eq. (11)] and of a normalized χ with 2 DOFs. This comparison highlights the differences between the proposed PDFs of the amplitude of each field component and the previous one ([27, eq. (11)]).

We note that the tail of PDF (15) has slightly lower values than the PDF (10) after about the abscissa of value 2. However, the PDF (15) has higher values than the PDF (10) from about the abscissa of value 0.5 to the 2 one. We note that the normalized χ distribution with 2 DOFs has the highest values of these PDFs from about the abscissa of value 0.65 to the 2 one.

Conversely, the PDF [27, eq. (11)], which is not correct, gives a higher probability for moderate values of abscissas (up to about an abscissa value of 0.6). Graphs of the CDFs related to the PDFs in Fig. 2 are not shown to save space.

In a similar way, we can calculate the PDF and CDF of the power received by the antenna inside the inner chamber. The powers can be considered RVs as is the case of the amplitudes of fields and equivalently of S_{21}. The power transmitted through the hole has a χ^2 distribution with 4 DOFs [33], [34] whereas the power distribution received by the antenna inside an RC has a χ^2 distribution with 2 DOFs when they operate in standalone way. We denote the RV representing the power transmitted through the hole by W_1. Inside the inner chamber, the power transmitted from the outer chamber is subject to a χ^2 distribution with 2 DOFs, which is the same as an exponential distribution [35]. We denote the RV representing such a power by Y_2. Accordingly, the power measured inside the inner chamber is obtained by the product of W_1 and Y_2. We can achieve the PDF and CDF of normalized RV

$$W_n = W_{1n} Y_{2n} = \frac{P_r}{P_t} = \left|S_{21,o,i}\right|_n^2 . \tag{17}$$

Therefore, we can write:

$$f_{W_{1n}}(w_{1n}) = 4 w_{1n} e^{-2w_{1n}} \tag{18}$$

$$f_{Y_{2n}}(y_{2n}) = e^{-y_{2n}} . \tag{19}$$

It follows:

$$f_{W_n}(w_n) = 4\sqrt{2}\sqrt{w_n} K_1\left(2\sqrt{2}\sqrt{w_n}\right), \tag{20}$$

$$F_{W_n}(w_n) = 1 - 4 w_n K_2\left(2\sqrt{2}\sqrt{w_n}\right). \tag{21}$$

C. ALTERNATIVE METHOD TO ACHIEVE THEORETICAL RESULTS

We note that (10) could also be achieved by manipulating (12) and the expression of the mean value of X, which is given by $\mu_X = \mu_{X_1}\mu_{X_2} = \frac{\pi}{2}\sigma_1\sigma_2$. Indeed, by setting $\mu_X = 1$ and replacing $\sigma_1\sigma_2 = \frac{2}{\pi}$ in (12), we achieve (10). This rationale could also be applied to achieve (11), (15), (16), (20) and (21) as they are derived from one parameter distributions. In other words, the same rationale of normalization applied on the starting PDFs in previous subsections could be applied to the nonnormalized PDFs and CDFs of the RVs X, Y and W. This alternative procedure could be useful only if the expressions of the nonnormalized PDFs and CDFs are explicitly known, as well as those of the related means, otherwise no advantage is obtained compared to the method used in this paper. Indeed, the integrals to be solved to achieve the nonnormalized theoretical results could also be harder. In our case, only the nonnormalized PDF corresponding to (10) was explicitly known, which is eq. (12) [26]. Therefore, the direct normalized approach is used as shown above.

D. COMPARISON METHODS USED FOR THE DISTRIBUTIONS

We need to compare experimental results from measurements to the theoretical ones. As mentioned above, we compare the distributions of the values of the field components normalized with respect to the mean values. It is specified that we do not know the theoretical mean values. Therefore, the normalization is performed from the theorical point of view as if we knew the theoretical mean, whereas the mean is estimated by measured data and used for the normalization of measured data themselves. For goodness-of-fit (GOF) tests, these cases are equivalent to those where some parameters of the theoretical PDF are estimated by measured data. A similar situation is found for a normal distribution in [36]. In the other words, GOF tests such as standard Kolmogorov-Smirnov (K-S) and Anderson-Darling (A-D) tests are unapplicable [36], [37], [38], [40], [41], [42]. These GOF tests can be applied, if the distributions of the statistics "d" and "A^2" are achieved by simulations for such two tests, respectively, as well as the relative critical values and/or p-value [36], [37], [38], [39], [40], [42]; i.e., these GOF tests can be applied by supporting the analysis with Monte-Carlo simulations. χ^2 for GOF test and relative p-value can be applied to any univariate distribution for which one can calculate the CDF [36], [39]. Since we have the availability of 50 measured samples for each frequency, we use the p-value from A-D test enhanced by Monte Carlo simulations. This test also gives more weight to the tails than does the K-S test [39]. However, by following the rationale shown in [42] and the suggestion by Stephen Senn in [43], we also used other tests and methods, whose results are only briefly discussed in this paper (see Sect. V below).

III. MEASUREMENT SETUP, DATA ACQUISITION AND PREPARATION

According to the abovementioned specifications, the scattering parameters $S_{21,o,i}$, $S_{21,o,o}$ and $S_{21,i,i}$ are the transmission coefficient between the chambers and those of the outer and inner chambers, respectively. The measurements of these three coefficients were performed over the frequency range (FR) from 1 GHz to 18 GHz, to compare theoretical and experimental distributions.

The measurements were performed in a cubic RC of 8 m^3 volume at the Università degli Studi di Napoli Parthenope,

where the input electromagnetic field is randomized by means of three metallic stirrers rotating in continuous mode as described in [25] and [44]. Random mechanical stirring (MS) due to the vibrations of the chamber walls under the effect of the motors of the stirrers improves the efficiency of the baseline MS. Figure 3 shows the inside of the RC where the inner chamber is visible.

(a) (b)

FIGURE 3. (a) Inside the RC where the inner chamber is well-visible. (b) Particular of the inner chamber where the coupling aperture is a slot of 32 mm × 2 mm.

The inner sizes of the inner chamber are exactly 473 mm × 473 mm × 473 mm. It has a removable side, which is exploited to change the coupling configuration. Specifically, a few and meaningful coupling apertures were used in our measurement campaigns.

The removable side was positioned on the flange of width of 40 mm of the inner chamber, which was covered by a sealing gasket. An ad-hoc stirrer was used as shown in Fig. 4(a) to acceptably achieve the assumed field distribution also at low frequencies of the FR. The stirrer, which works in continuous mode, includes a vertical prism, metalized by adhesive aluminium except for the top wall.

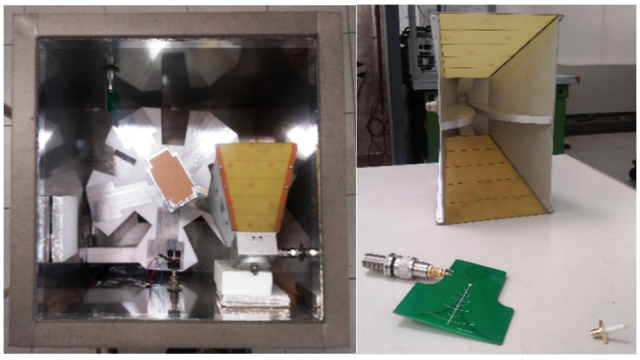

(a) (b)

FIGURE 4. Inner chamber configurations. (a) Stirrer ad hoc built including a metalized rectangular prism. (b) Antennas used for measurements.

The apertures were created by cutting off parts of aluminium slabs, which were used as removable side. These interchangeable aluminium slabs can be considered as test samples, which were properly placed on the top of the inner chamber. The ES apertures had rectangular slot shape of 20 mm × 2 mm and 32 mm × 2 mm, as well as a circular hole shape of 16 mm and 32 mm in diameter.

With reference to the set-up in Fig. 1, the antennas $A_{drwh,o}$ and $A_{drwh,i}$ were ETS-Lindgren 3115 double-ridge waveguide horn antennas; the FR of such antennas ranges from 1 GHz to 18 GHz. Since the coupling aperture were small, no potential direct coupling from the aperture to the antennas inside the inner chamber can significantly affect the measurements. Note that under the abovementioned assumptions on the stirring of the fields inside the two chambers, the position of the coupling aperture on the walls of the inner chamber does not affect the results. The other two antennas were ultra-wideband image transmission TEM antennas (model XR 170); in Fig. 1, they are denoted by A_o and A_i. The FR of such antennas ranges from 1.4 GHz to 10.5 GHz. We denote these antennas by I-T-TEM antennas in the text. All the antennas used in the measurements are linearly polarized. However, since the I-T-TEM antennas were operated outside their intrinsic FR, we performed some measurements by replacing them with two equal dipole antennas shown in Fig. 4(b). These results were not shown for brevity. However, they allowed us to check that the I-T-TEM antennas behave as linearly polarized antennas when they work over the whole used FR. Fig. 4(b) shows the antennas used for measurements. The dipoles antennas have SMA connectors with straight terminals. The measurement set-up includes a two-port Agilent 8363B vector network analyzer (VNA).

The measurements were performed up to 18 GHz to show the effect of the electromagnetic behaviour of the apertures on the distribution of the field components inside the inner chamber, which changes from ES to EL, by crossing the resonance region, according to the ratio between the size of the apertures and the wavelength over the FR. Such an effect entails a change of the distribution of the field components as shown below. In particular, considering the apertures used in the measurements, we show that the distributions of the field change from one concerning an ES aperture to another concerning an EL aperture over the FR.

A. DATA ACQUISITION AND DATA PREPARATION

In the measurements, 1700 uniformly distributed samples over the whole FR from 1 GHz to 18 GHz were acquired for each frequency sweep. Fifty frequency sweeps were acquired for each of the three measured scattering parameters. A step frequency (SF) of 10 MHz was used. Considering the spread of the spectrum of the signal inside the RC [44], the width of the intermediate frequency filter bandwidth (IFBW) was set to 2 kHz. Acquired samples can be represented by a matrix of 1700 columns (frequency points) and 50 rows (frequency sweeps) so that the frequency is constant for each column. Hence, 50 uncorrelated samples were acquired for each of the 1700 frequency points. Specifically, 1700 set of 50 uncorrelated samples each corresponding to different frequency points were considered for data processing. Therefore, we achieved and tested 1700 CDFs of the normalized $|S_{21,o,i}|$. The results are presented for each of the used coupling apertures. Some verification tests

were performed on the normalized $|S_{21,i,i}|$ and $|S_{21,o,o}|$ to check if the necessary conditions on the distributions of the fields inside the single chambers were acceptably met. The possible biases of the real and imaginary parts were removed frequency by frequency. Consequently, the samples to be processed were also independent. Moreover, the amplitudes of the samples of each group were normalized to the relative average values.

It is specified that the uncorrelation of the acquired samples was checked by Pearson's autocorrelation coefficient and autocorrelation function. Finally, by SE of the inner chamber (enclosure), which is obtained by measurements, the assumed isolation conditions were verified [1], [13], [14], [16], [22], [23]. Results are not shown here for brevity.

IV. EXPERIMENTAL RESULTS

In this section, we show the comparisons between theoretical and experimental CDFs by p-value from A-D test. We specify that no statistical difference was found in the results when the different abovementioned antennas were used in the measurements. For $|S_{21,o,i}|$, the comparisons are also shown by considering the theoretical CDF achieved in [27, eq. (12)]. We recall that all the tests were performed on 50 samples for each of the 1700 frequency points.

It is specified that only comparisons from the filed component distributions (RVs X, Y) are shown in the paper. However, it is highlighted the results from comparisons using the power ratios exactly lead to the same conclusions. In order to simplify the reading of the results, they are presented by a mapping of the p-values, which represent the probability value from the test for each frequency point. Therefore, the map of the p-values gives an overview of the results for each configuration of coupling between the chambers. Moreover, an horizontal line representing the threshold at the 5% of significance level further helps the reading of the results.

A. SINGLE ES APERTURES FILTERING A SINGLE FIELD COMPONENT (1D CASES)

In this subsection, the results regarding the two cases of single apertures filtering a single component of the field are shown: the slot of 20 mm × 2 mm and the one of 32 mm × 2 mm. We check the distributions of the field components in the two chambers when they operate in a standalone way as they are essential to test the theoretical results obtained in Sect. II. In these two cases (inner and outer chamber), the theoretical CDF is a normalized χ with 2 DOFs. Figures 5 and 6 show the p-value for the normalized amplitude of S_{21} measured inside the internal chamber and inside outer chamber, respectively. In these measurements, the inner chamber was inside the outer chamber and the coupling aperture wase of 32 mm × 2 mm.

For the inner chamber (Fig. 5), the theoretical hypothesis was rejected at the 5% and 1% of significance levels; the rejection rates were 10.5% and 3.1%, respectively. Note that

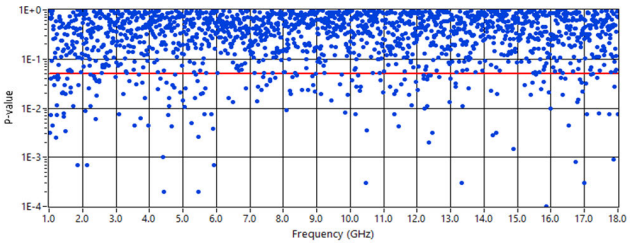

FIGURE 5. P-value from A-D test of 50 samples on the normalized amplitude of $S_{21,i,i}$. The coupling aperture was the slot of 32 mm x 2 mm. The theoretical CDF is a normalized χ distribution with 2 DOFs.

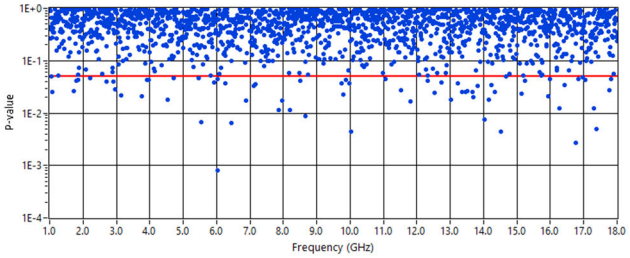

FIGURE 6. P-value from A-D test of 50 samples on the normalized amplitude of $S_{21,o,o}$. The theoretical CDF is a normalized χ distribution with 2 DOFs.

the red line represents the threshold at the 5% of significance level as mentioned above.

For the outer chamber (Fig. 6), the theoretical hypothesis was accepted both at the 5% and 1% of significance levels as expected; in this case, the rejection rates were of 4.1% and 0.5%, respectively.

The rejection of the test on the distribution of the amplitude of the field components inside the inner chamber was likely because of an ordinary imperfect stirring inside the inner chamber due to the limited volume and only to the use of MS. Such an imperfection was rather generalized over the entire FR even though it was more significant at the lower frequencies as expected. However, the map of the p-values and the rates of the reject of the test show that results are acceptable for the comparisons in the paper.

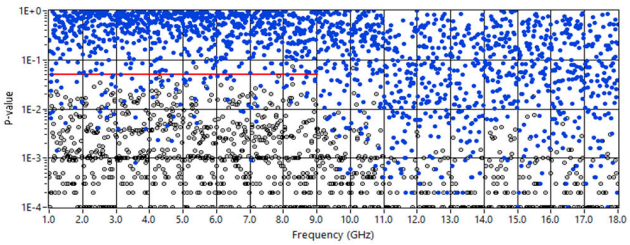

FIGURE 7. P-value from A-D test of 50 samples on the normalized amplitude of $S_{21,o,i}$. The coupling aperture was the slot of 20 mm x 2 mm. The theoretical CDF is a normalized double Rayleigh (eq. 11) for the blue and full circle and the CDF in [27, eq. (12)] for the black and empty circle.

Figure 7 and 8 show results of the p-value for $|S_{21,o,i}|$, under the hypothesis that the theoretical CDF is a normalized double Rayleigh (eq. 11), in case where the coupling aperture

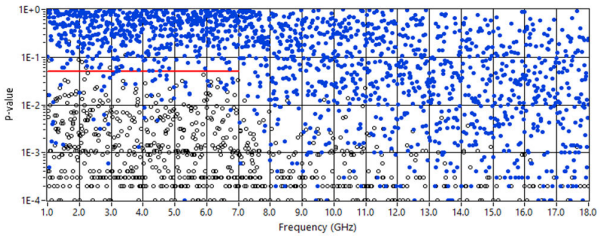

FIGURE 8. P-value from A-D test of 50 samples on the normalized amplitude of $S_{21,o,i}$. The coupling aperture was the slot of 32 mm x 2 mm. The theoretical CDF is a normalized double Rayleigh (eq. 11) for the blue and full circle and the CDF in [27, eq. (12)] for the black and empty circle.

are the slots of 20 mm × 2 mm and 32mm × 2 mm, respectively. Fig. 7 and 8 also show results of the p-value under the hypothesis that the theoretical distribution is the CDF [27, eq. (12)].

For the slot of 20 mm (Fig. 7), the cut off frequency is 7.5 GHz. However, the A-D test was performed over the sub-FR from 1 GHz to 9 GHz for the normalized double Rayleigh distribution. The theoretical hypothesis was rejected at the 5% and 1% of significance levels; the rejection rates were 10.4% and 2.9%, respectively.

The theoretical CDF [27, eq. (12)] was rejected at the 5% and 1% of significance levels over the same sub-FR from 1 GHz to 9 GHz; the rejection rates were 99.6% and 86.1%, respectively. Note that the results in [27, eqs (11) and (12)] were obtained regardless of the form and size of the coupling aperture; however, we note that the rejection rates (p-value map) strongly worsen for frequencies from 9 GHz to 18 GHz. It is specified that p-values were mapped to 10^{-4} for plotting and numerous rejected samples concerning the theoretical CDF [27, eq. (12)] are not visible.

Results in Fig. 8 are coherent with those in Fig. 7. In this case, the cut off frequency of the slot of 32 mm is about 4.7 GHz. The A-D test was performed over the sub-FR from 1 GHz to 7 GHz for the normalized double Rayleigh distribution. The theoretical hypothesis was rejected at the 5% and 1% of significance levels; the rejection rates were 8.5% and 3.0%, respectively.

The theoretical CDF [27, eq. (12)] was rejected at the 5% and 1% of significance levels over the same FR from 1 GHz to 7 GHz; the rejection rates were 98.7% and 89%, respectively. Again, note that the rejection rates (p-value map) strongly worsen for frequencies higher than 7 GHz.

Note that the rejection rates in the Fig. 7 and 8 are totally compatible with those due to imperfect stirring inside inner chamber (see Fig. 5). Therefore, even though the test was rejected at the 5% and 1% of significance levels for these apertures, the rejection ratios and the p-value maps show that the experimental and theoretical CDFs match well. Moreover, the visible migration toward a different distribution is also expected for the electromagnetic behaviour of the two apertures, which *de facto* represents the real physical problem.

It is important to note that the distribution [27, eqs. (11) and (12)] is totally unsuitable to represent the distribution of the field for these apertures across the entire FR.

We specify that the tests in this paper were performed up to more than the cut off frequency of the coupling aperture as the results were reasonable and acceptable up to about the considered frequencies. We also specify that results led to the same conclusion when FS was considered in data set. Actually, the results gradually worsened in terms of rejection rate with the increasing of the FS bandwidth (FSB) as expected. This behaviour in the results of the tests was not present for an EL coupling aperture. It is due to the fact that FS is not included in the development of the theoretical models. Note that several results were not shown in the paper for brevity. However, even though theoretical models do not include the FS effect, it was verified that the use of FSBs of the order of some hundred MHz led to the same conclusions.

B. SINGLE ES APERTURES FILTERING TWO FIELD COMPONENTS (2D CASES)

In this subsection, results regarding the two cases of single ES apertures filtering two field components are shown. Single ES circular apertures were used for ease of practical realization; however, the same results are obtained if different forms of 2D coupling apertures are used. The coupling apertures were two holes of 16 and 32 mm in diameter. It is specified that results for the normalized amplitude of $S_{21,i,i}$ inside the internal chamber are the same as those in Fig. 5 except for the intrinsic statistical fluctuation. They are not shown to save space.

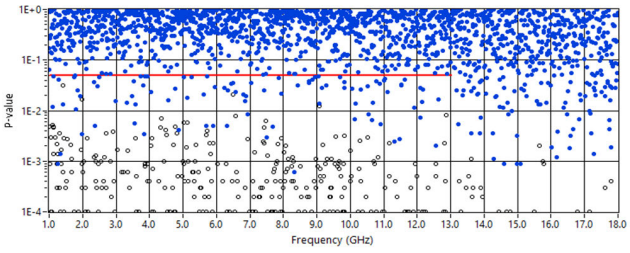

FIGURE 9. P-value from A-D test of 50 samples on the normalized amplitude of $S_{21,o,i}$. The coupling aperture was the hole of 16 mm in diameter. The theoretical CDF is given by (16) for the blue and full circle and the CDF in [27, eq. (12)] for the black and empty circle.

Figure 9 shows the p-values from the comparison between the theoretical CDF given by (16) and the normalized amplitude of $S_{21,o,i}$, where the aperture is the hole of 16 mm in diameter.

For a circular hole of 16 mm in diameter, the cut off frequency is about 11 GHz. However, the A-D test was performed over the sub-FR from 1 GHz to 13 GHz. The theoretical hypothesis was rejected at the 5% and 1% of significance levels; the rejection rates were 7.8% and 1.8%, respectively.

The theoretical CDF [27, eq. (12)] was rejected at the 5% and 1% of significance levels over the same sub-FR

from 1 GHz to 13 GHz; the rejection rates were 100% and 99.7%, respectively. Again, note that the rejection rates (p-value map) strongly worsen for frequencies higher than 13 GHz.

Figure 10 shows the p-value from the comparison between the theoretical CDF given by (16) and the normalized amplitude of $S_{21,o,i}$, where the aperture is the hole of 32 mm in diameter.

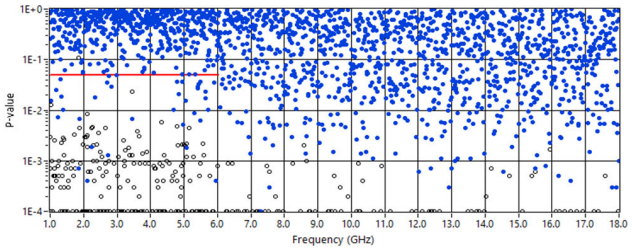

FIGURE 10. P-value from A-D test of 50 samples on the normalized amplitude of $S_{21,o,i}$. The coupling aperture was the hole of 32 mm in diameter. The theoretical CDF is given by (16) for the blue and full circle and the CDF in [27, eq. (12)] for the black and empty circle.

For a circular hole of 32 mm in diameter, the cut off frequency is about 5.5 GHz. However, the A-D test was performed over the sub-FR from 1 GHz to 6 GHz. The theoretical hypothesis was rejected at the 5% and 1% of significance levels; the rejection rates were 7% and 2.4%, respectively.

The theoretical CDF [27, eq. (12)] was rejected at the 5% and 1% of significance levels over the same sub-FR from 1 GHz to 6 GHz; the rejection rates were 99.8% and 99.4%, respectively. Again, note that the rejection rates (p-value map) strongly worsen for frequencies higher than 6 GHz.

Again, we note that the rejection rates in the Fig. 9 and 10 are totally compatible with those due to imperfect stirring in the inner chamber (see Fig. 5). Therefore, even though the test was rejected at the 5% and 1% of significance levels for these apertures, the rejection ratios and the p-value maps show that the experimental and theoretical CDFs match well. Moreover, the visible migration toward a different distribution is also expected for the electromagnetic behaviour of the two apertures, which *de facto* represents the real physical problem.

It is important to note that the distribution [27, eqs. (11) and (12)] is totally unsuitable to represent the distribution of the field for these apertures across the entire FR.

C. EFFECTS OF THE BEHAVIOUR OF AN APERTURES FROM ES TO EL

We also verified that the normalized χ distribution with 2 DOFs is totally unsuitable to represent the distribution of the field components inside the inner chamber for a single ES coupling aperture. However, with increasing the frequency, the distribution of the field components moves gradually toward such a distribution according to the ratio between wavelength and size of the coupling aperture. Such an electromagnetic behaviour can clearly be seen from the results shown in Fig. 11, which concern the hole of 32 mm in diameter. Fig. 11 shows the results of the p-value from the comparison between theoretical and experimental CDFs, where the former is a normalized χ distribution with 2 DOFs. The theoretical hypothesis was rejected at the 5% and 1% of significance levels over the sub-FR higher than 8 GHz; the rejection rates were 7.5% and 2.7%, respectively.

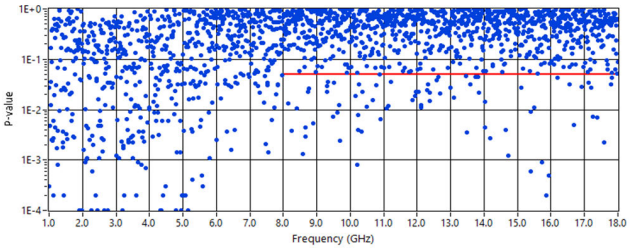

FIGURE 11. P-value from A-D test of 50 samples on the normalized amplitude of $S_{21,o,i}$. The coupling aperture was the hole of 32 mm in diameter. The theoretical CDF is a normalized χ distribution with 2 DOFs.

Hence, by the map of the p-value, we showed the migration of the distribution of the amplitude of the field components inside the inner chamber toward a χ distribution with 2 DOFs with increasing frequency.

The results in Fig. 11 confirm the theory in [27] on the expected statistics for the field components inside the enclosure when the coupling apertures is EL and the fields inside the two chambers are still independent.

Fig. 11 also shows that the distribution of the components of the field inside the inner chamber in the measurements of SE of materials and gaskets could not be a χ distribution with 2 DOFs at the low frequencies of the working FR of the aperture regardless of the volume of the inner chamber. Such low frequencies could correspond to a part of the resonance region of the coupling aperture according to sizes of the aperture itself [1, pag. 74, note 1], [11], [13], [14], [16]. Hence, at the low frequencies, the distribution of the components of field inside the inner chamber could be affected by both the size of the coupling aperture and volume of the inner chamber itself. Such two causes are independent; the latter produces resonance phenomenon inside the volume of the inner chamber, whose effects were shown in [23], where the distribution of the field inside the enclosures was expected to be a χ distribution with 2 DOFs being connected to leakage. For the former cause, notable differences in the measurements of SE could be obtained, when a measurement model including the ratio between maximum values is used, for both SE measurements of materials and gaskets [1], [22, Subsection I-D] and SE of enclosures. Indeed, such maximum values (the one in the numerator and that in the denominator of the ratio) could come from different distributions. The abovementioned former cause includes both the size and the form of the coupling aperture (or apertures) for the SE of enclosure. Even though measurements model on SE

of materials and gaskets in [1, Annex G] is inefficient [14], [22], it can be improved by also considering the ratio between maximum values [22, Subsection I-D]. The ratio between maximum values $\left(\left|S_{21,o,o}\right|^2\right)_N^{Max} \Big/ \left(\left|S_{21,o,i}\right|^2\right)_N^{Max}$, where the superscript "Max" and the subscript "N" mean that the maximum value is taken among N samples, which represents the SE of the enclosure [1], [23], would tend to reduce the estimate of the SE for both enclosures and materials and gaskets, when the distribution of the denominator has values concerning the tails greater than the χ distribution with 2 DOFs. Note that no affectation would be present for the so-called SE_4 measurement model [11, eq. (14)], [16, eq. (15)], [22, Fig. 12 and 13], if the ratio between the maximum values were used in SE measurements of materials and gaskets. Hence, we note that the distributions found inside the inner chamber have a conservative effect on the estimates of SE for both enclosures and materials and gaskets, when a measurement model including the ratio between maximum values is used. However, they reveal a higher probability of high values of field inside an enclosure according to the ES coupling aperture. This is relevant in electromagnetic compatibility. On the other hand, since the conservative estimation of SE is subject to the statistical fluctuations, the higher probability of high values of field inside an enclosure is however a warning.

V. DISCUSSION

The results presented in this work confirms findings achieved through alternative methods, i. e., the rationale in [42] and the suggestion by Stephen Senn in [43] were followed. Such results are not shown in the paper for brevity. The p-values achieved from K-S test (which is enhanced by Monte Carlo simulations as mentioned above) on the same measurement datasets used in the paper led to the same conclusions. The p-value from χ^2 for GOF, as well as from A-D and K-S tests, performed on different datasets, obtained by the same measurements, by considering FS and consequently a greater number of independent samples, led to the same conclusions, albeit with the limitation on FS mentioned above. Also, the results from the comparison between theoretical and experimental CDFs [45] by mean square error still led to the same conclusions.

Results from measurements where different antennas were used, shown in Fig. 4(b), led to the same conclusions.

It should be highlighted that the mathematical models were developed under the assumption that the fields inside both the chambers are perfectly stirred, i.e., each sample acquired inside the inner chamber was produced both by internal and external stirring. It is worth noticing that the results in this paper do not contradict the results in [19, Fig. 6(b)] as the internal stirrer was fixed in the latter case.

Concerning the results in [28, Table 2], we found a difference with the expectation calculated in in [27]. They also disagree with the result shown in this paper for a large coupling aperture. Indeed, the expected result was a Rayleigh distribution (the size of the coupling aperture was 1 m × 1 m, [6, Fig. 6]), but a double Rayleigh was found instead. Only the isolation between the chambers was mentioned to justify the results achieved.

About the inconsistent results at the frequencies 3 and 4 GHz in [26, Fig.5d], we think that the reason was the low stirring efficiency inside the enclosure, i.e., considering the shorter dimension of the enclosure (0.12 m) and only the use of FS, probably, the stirring was imperfect inside the enclosure. In other words, an ideal Rayleigh distribution was not achieved inside the enclosure up to frequencies about of 4 GHz for the amplitude $\left|S_{21,i,i}\right|$, when it worked in a standalone way and only FS was used.

Finally, we stress that the theoretical models found and verified in this paper is derived from physical basis. This aspect is very important as discussed in [43, pag. 152].

VI. CONCLUSION

We studied the statistical distribution of the amplitude of the field components inside the inner chamber of NRCs, as well as inside the RC fed by the other chamber for ARCs. The results are applicable to electrically large enclosures, as well as to fixtures for SE measurement of materials and gaskets in RCs. We showed the correct procedures to achieve the normalized distributions of the amplitude of the field components, which are useful for SE measurements of enclosures with a single and ES aperture. For the first time, we showed that it is necessary to distinguish between the apertures that filter a single component of the field (1D apertures) and those that filter two components of the field (2D apertures). We provided novel normalized distributions of the amplitude of the field components for basic cases of single and electrically small coupling 1D and 2D apertures. The novel distributions showed a higher probability of high values of the field inside an enclosure according to the electrically small coupling aperture. We found that the leakage of the inner chamber has not affected the results from the aperture used in these measurements. Based on this study, extensions to two or more independent apertures can easily developed.

ACKNOWLEDGMENT

The authors thank Dr. Giovanni Morieri of the Geotechnical Engineering Laboratory, Engineering Department, University of Naples Parthenope, for kind assistance in the preparation of tested samples.

REFERENCES

[1] *Electromagnetic Compatibility (EMC), Part 4–21: Testing and Measurement Techniques—Reverberation Chamber Test Methods*, Standard IEC 61000-4-21, Int. Electrotechnical Commission, Geneva, Switzerland, 2011.

[2] *CTIA Test Plan for Wireless Device Over-the-Air Performance, V.4.0 'Test Methodology, SISO, Reverberation Chamber'*, document 01.21, CTIA Certification, Washington, DC, USA, 2022.

[3] *CTIA Test Plan for Wireless Device Over-the-Air Performance, V.4.0.2, Document 01.73 'Supporting Procedures,' Section 6 'Reverberation-Chamber Precharacterization Procedure'*, document 01.73, CTIA Certification, Washington, DC, USA, Mar. 2022.

[4] *Technical Specification Group Radio Access Network; Radio Frequency (RF) Conformance Testing Background for Radiated Base Station (BS) Requirements (Release 17)*, document TR37.941, v17.0.0, 3GPP, Valbonne, France, Mar. 2022.

[5] C. L. Holloway, D. A. Hill, M. Sandroni, J. M. Ladbury, J. Coder, G. Koepke, A. C. Marvin, and Y. He, "Use of reverberation chambers to determine the shielding effectiveness of physically small, electrically large enclosures and cavities," *IEEE Trans. Electromagn. Compat.*, vol. 50, no. 4, pp. 770–782, Nov. 2008.

[6] A. Gifuni, A. Sorrentino, A. Fanti, G. Ferrara, M. Migliaccio, G. Mazzarella, and F. Corona, "On the evaluation of the shielding effectiveness of an electrically large enclosure," *Adv. Electromagn.*, vol. 1, no. 1, pp. 84–91, 2012.

[7] A. C. Marvin, I. D. Flintoft, J. F. Dawson, M. P. Robinson, S. J. Bale, S. L. Parker, M. Ye, C. Wan, and M. Zhang, "Enclosure shielding assessment using surrogate contents fabricated from radio absorbing material," in *Proc. Asia–Pacific Int. Symp. Electromagn. Compat. (APEMC)*, Shenzhen, China, May 2016, pp. 994–996.

[8] I. D. Flintoft, S. J. Bale, A. C. Marvin, M. Ye, J. F. Dawson, C. Wan, M. Zhang, S. L. Parker, and M. P. Robinson, "Representative contents design for shielding enclosure qualification from 2 to 20 GHz," *IEEE Trans. Electromagn. Compat.*, vol. 60, no. 1, pp. 173–181, Feb. 2018.

[9] A. Gifuni, G. Ferrara, M. Migliaccio, and A. Sorrentino, "Estimate of the shielding effectiveness of an electrically large enclosure made with pierced metallic plate in a well-stirred reverberation chamber," *Prog. Electromagn. Res. C*, vol. 44, pp. 133–144, 2013.

[10] M. O. Hatfield, "Shielding effectiveness measurements using mode-stirred chambers: A comparison of two approaches," *IEEE Trans. Electromagn. Compat.*, vol. 30, no. 3, pp. 229–238, Aug. 1988.

[11] C. L. Holloway, D. A. Hill, J. Ladbury, G. Koepke, and R. Garzia, "Shielding effectiveness measurements of materials using nested reverberation chambers," *IEEE Trans. Electromagn. Compat.*, vol. 45, no. 2, pp. 350–356, May 2003.

[12] *IEEE Standard Method for Measuring the Effectiveness of Electromagnetic Shielding of Enclosures and Boxes Having All Dimensions Between 0.1 M and 2 M*, Standard IEEE Std 299.1, New York, NY, USA, 2013.

[13] A. Gifuni and M. Migliaccio, "Use of nested reverberating chambers to measure shielding effectiveness of nonreciprocal samples taking into account multiple interactions," *IEEE Trans. Electromagn. Compat.*, vol. 50, no. 4, pp. 783–786, Nov. 2008.

[14] A. Gifuni, "A proposal to improve the standard on the shielding effectiveness measurements of materials and gaskets in a reverberation chamber," *IEEE Trans. Electromagn. Compat.*, vol. 59, no. 2, pp. 394–403, Apr. 2017.

[15] V. M. Primiani, F. Moglie, and A. P. Pastore, "Field penetration through a wire mesh screen excited by a reverberation chamber field: FDTD analysis and experiments," *IEEE Trans. Electromagn. Compat.*, vol. 51, no. 4, pp. 883–891, Nov. 2009.

[16] A. Gifuni, G. Gradoni, C. Smartt, S. Greedy, A. M. Villalón, L. Bastianelli, F. Moglie, V. Mariani Primiani, S. Perna, and D. Thomas, "Latest developments on the shielding effectiveness measurements of materials and gaskets in reverberation chambers," *IET Sci., Meas. Technol.*, vol. 14, no. 4, pp. 435–445, Jun. 2020, doi: 10.1049/iet-smt.2019.0242.

[17] V. Gkatsi, R. Vogt-Ardatjew, H. Schipper, and F. Leferink, "Board level shielding effectiveness measurements using the dual VIRC," in *Proc. Asia–Pacific Int. Symp. Electromagn. Compat. (APEMC)*, Sep. 2021, pp. 1–4, doi: 10.1109/APEMC49932.2021.9596719.

[18] S. van de Beek, R. Vogt-Ardatjew, H. Schipper, and F. Leferink, "Vibrating intrinsic reverberation chambers for shielding effectiveness measurements," in *Proc. Int. Symp. Electromagn. Compat.*, Sep. 2012, pp. 1–6, doi: 10.1109/EMCEUROPE.2012.6396655.

[19] N. Nourshamsi, J. C. West, C. E. Hager, and C. F. Bunting, "Generalized extreme value distributions of fields in nested electromagnetic cavities," *IEEE Trans. Electromagn. Compat.*, vol. 61, no. 4, pp. 1337–1344, Aug. 2019.

[20] T. H. Lehman and G. J. Freyer, "Characterization of the maximum test level in a reverberation chamber," in *Proc. IEEE Int. Symp. Electromagn. Compat.*, Austin, TX, USA, Aug. 1997, pp. 44–47.

[21] A. Gifuni, "Deterministic approach to estimate the upper bound of the electric field in a reverberation chamber," *IEEE Trans. Electromagn. Compat.*, vol. 53, no. 3, pp. 570–578, Aug. 2011, doi: 10.1109/TEMC.2010.2102359.

[22] A. Gifuni, G. Gradoni, R. Serra, G. Grassini, M. Adil, A. Buono, F. Nunziata, and M. Migliaccio, "On the improvement of shielding effectiveness measurements of materials and gaskets in reverberation chambers," *IEEE Trans. Electromagn. Compat.*, vol. 64, no. 5, pp. 1653–1664, Oct. 2022, doi: 10.1109/TEMC.2022.3193191.

[23] A. Gifuni, L. Bastianelli, G. Gradoni, F. Moglie, S. Perna, C. Smartt, and V. M. Primiani, "On the shielding effectiveness calculation of enclosures through measurements in reverberation chambers," *IEEE Trans. Electromagn. Compat.*, vol. 63, no. 5, pp. 1395–1406, Oct. 2021, doi: 10.1109/TEMC.2021.3057449.

[24] J. G. Kostas and B. Boverie, "Statistical model for a mode-stirred chamber," *IEEE Trans. Electromagn. Compat.*, vol. 33, no. 4, pp. 366–370, Nov. 1991.

[25] P. Corona, G. Ferrara, and M. Migliaccio, "Reverberating chambers as sources of stochastic electromagnetic fields," *IEEE Trans. Electromagn. Compat.*, vol. 38, no. 3, pp. 348–356, Aug. 1996.

[26] Y. He and A. C. Marvin, "Aspects of field statistics inside nested frequency-stirred reverberation chambers," in *Proc. IEEE Int. Symp. Electromagn. Compat.*, Austin, TX, USA, Aug. 2009, pp. 171–176.

[27] M. Höijer and L. Kroon, "Field statistics in nested reverberation chambers," *IEEE Trans. Electromagn. Compat.*, vol. 55, no. 6, pp. 1328–1330, Dec. 2013, doi: 10.1109/TEMC.2013.2249510.

[28] W. Qi, K. Chen, X. Shen, Y. Zhao, Q. Xu, T. H. Loh, and Y. Huang, "Statistical analysis for shielding effectiveness measurement of materials using reverberation chambers," *IEEE Trans. Electromagn. Compat.*, vol. 65, no. 1, pp. 17–27, Feb. 2023, doi: 10.1109/TEMC.2022.3223996.

[29] Y. Rahmat-Samii and R. Mittra, "Electromagnetic coupling through small apertures in a conducting screen," *IEEE Trans. Antennas Propag.*, vol. AP-25, no. 2, pp. 180–187, Mar. 1977, doi: 10.1109/TAP.1977.1141554.

[30] C. M. Butler, Y. Rahmat-Samii, and R. Mittra, "Electromagnetic penetration through apertures in conducting surfaces," *IEEE Trans. Antennas Propag.*, vol. AP-26, no. 1, pp. 82–93, Jan. 1978.

[31] D. A. Hill, M. T. Ma, A. R. Ondrejka, B. F. Riddle, M. L. Crawford, and R. T. Johnk, "Aperture excitation of electrically large, lossy cavities," *IEEE Trans. Electromagn. Compat.*, vol. 36, no. 3, pp. 169–178, Aug. 1994.

[32] T. H. Leman, "A statistical theory of electromagnetic fields in complex cavities," EMP, Tech. Rep. 494, May 1993.

[33] D. A. Hill, "Electromagnetic theory of reverberation chambers," U.S. Natl. Inst. Stand. Technol., Boulder, CO, USA, Tech. Rep., 1506, 1998.

[34] J. Ladbury, G. Koepke, and D. Camell, "Evaluation of the NASA Langley research center mode-stirred chamber facility," Nat. Inst. Standards Technol., Boulder, CO, USA, Tech. Rep., 1508, Jan. 1999.

[35] A. Papoulis, *Probability, Random Variables and Stochastic Process*. New York, NY, USA: McGraw-Hill, 1991.

[36] M. A. Stephens, "Asymptotic results for goodness-of-fit statistics with unknown parameters," *Ann. Statist.*, vol. 4, no. 2, pp. 357–369, Mar. 1976.

[37] H. W. Lilliefors, "On the Kolmogorov–Smirnov test for normality with mean and variance unknown," *J. Amer. Stat. Assoc.*, vol. 62, no. 318, pp. 399–402, Jun. 1967, doi: 10.2307/2283970.

[38] H. W. Lilliefors, "On the Kolmogorov–Smirnov test for the exponential distribution with mean unknown," *J. Amer. Stat. Assoc.*, vol. 64, no. 325, pp. 387–389, Mar. 1969.

[39] (2023). *NIST/SEMATECH E-Handbook of Statistical Methods*. [Online]. Available: http://www.itl.nist.gov/div898/handbook/

[40] F. J. Massey, "The Kolmogorov–Smirnov test for goodness of fit," *J. Amer. Stat. Assoc.*, vol. 46, no. 253, pp. 68–78, Mar. 1951.

[41] C. Lemoine, P. Besnier, and M. Drissi, "Investigation of reverberation chamber measurements through high-power goodness-of-fit tests," *IEEE Trans. Electromagn. Compat.*, vol. 49, no. 4, pp. 745–755, Nov. 2007.

[42] R. L. Wasserstein and N. A. Lazar, "The ASA statement on p-values: Context, process, and purpose," *Amer. Statistician*, vol. 70, no. 2, pp. 129–133, Apr. 2016, doi: 10.1080/00031305.2016.1154108.

[43] R. Nuzzo, "Scientific method: Statistical errors," *Nature*, vol. 506, no. 7487, pp. 150–152, Feb. 2014, doi: 10.1038/506150a.

[44] P. Corona, G. Ferrara, and M. Migliaccio, "A spectral approach for the determination of the reverberating chamber quality factor," *IEEE Trans. Electromagn. Compat.*, vol. 40, no. 2, pp. 145–153, May 1998.

[45] L. R. Arnaut, "Compound exponential distributions for undermoded reverberation chambers," *IEEE Trans. Electromagn. Compat.*, vol. 44, no. 3, pp. 442–457, Aug. 2002.

ANGELO GIFUNI (Member, IEEE) received the Laurea degree in nautical science from Università degli Studi di Napoli "Parthenope," Naples, Italy, in 1998. He is currently the Head of the Experimental Electromagnetism Laboratory, Department of Engineering, Università degli Studi di Napoli "Parthenope." His main research interest includes applied electromagnetics.

ANETT KENDERES received the master's degree in electrical engineering from the Budapest University of Technology and Economics, while spending a year at the Technical University of Munich. She is currently pursuing the Ph.D. degree with the cooperative degree program jointly held by the Department of Broadband Infocommunications and Electromagnetic Theory, Budapest University of Technology, and by company Robert Bosch (Mobility Electronics/Electromagnetic Compatibility). During the Ph.D. studies, she was a visiting student at the Parthenope University of Naples. During the past years, she gained experience in the application fields of electromagnetic compatibility, sensitivity analysis, and applied superconductivity. Her research interest includes numerical methods utilized to solve computational electromagnetics-related problems.

GIUSEPPE GRASSINI was born in Naples, Italy, in 1959. He has been an Electronics and Electroacoustic Expert with the Department of Engineering, Università degli Studi di Napoli "Parthenope," Naples, since 1989.

ANDREA BUONO (Senior Member, IEEE) was born in Naples, Italy, in 1984. He received the B.Sc. and M.Sc. degrees and the Ph.D. degree in information engineering from Università degli Studi di Napoli "Parthenope," Naples, in 2010, 2013, and 2017, respectively. Since 2018, he has been an Assistant Professor with Università degli Studi di Napoli "Parthenope." His main research interest includes applied electromagnetics.

GABRIELE GRADONI (Member, IEEE) received the Ph.D. degree in electromagnetics from Università Politecnica delle Marche, Ancona, Italy, in 2010. In 2008, he was a Visiting Researcher with the Time, Quantum, and Electromagnetics Team, National Physical Laboratory, Teddington, U.K. From 2010 to 2013, he was a Research Associate with the Institute for Research in Electronics and Applied Physics, University of Maryland, College Park, MD, USA. From 2013 to 2016, he was a Research Fellow with the School of Mathematical Sciences, University of Nottingham, U.K., where he became a Full Professor of electromagnetics engineering and applied mathematics, in 2022. Since 2023, he has been a Chair Professor of wireless and satellite communications with the University of Surrey, U.K., an Adjunct Professor with the University of Illinois at Urbana–Champaign, USA, and a Visiting Fellow with the University of Cambridge, U.K. His main research interests include quantum computing and electromagnetics channel modeling for integrated sensing and communications.

Open Access funding provided by 'Università degli Studi di Napoli "Parthenope"' within the CRUI CARE Agreement